URSI AP-RASC, Sydney, Australia, 17 – 22 August 2025

Broadband self-holography of EDA2 - an SKA-Low prototype station

Jishnu N. Thekkeppattu*(1), Marcin Sokołowski(1), and Randall B. Wayth(2)(1)
(1) International Centre for Radio Astronomy Research (ICRAR), Curtin University, Bentley, WA 6102, Australia
(2) SKA Observatory, 26 Dick Perry Avenue, Kensington WA 6151, Australia

Abstract

In this paper we present results from a broadband version of phased array self-holography and demonstrate it using actual data from an SKA-Low prototype station EDA2. We find that the broadband self-holography using raw voltages yields results consistent with `mfcal` which is a conventional visibility based technique. We also find that the effects of RFI are minimal in holographic calibration, owing to the formation of a reference beam towards the calibrator source which isolates it from rest of the interfering sources. We show that broadband self-holography is an attractive alternative to `mfcal` for station calibration.

1 Introduction

Due to its inherent simplicity and scalability, holographic calibration of large-N phased array radio telescopes has gathered considerable attention as an alternative to visibility based techniques[1, 2, 3, 4, 5]. However, most of this has been spot frequency measurements, while the modern large-N phased array systems, such as the SKA-Low, are designed to be broadband. In this paper, we extend the mathematics for spot frequency self-holography presented in [5] by including a frequency axis. We test this broadband version using data from EDA2, an SKA-Low prototype station [6].

2 Mathematical background

We start with set of channelised voltages denoted by $v_{\tau\eta\nu}$, where η is the antenna index, ν is the frequency index and τ is the time index. Here, the term "antenna" includes the physical antenna, as well as the associated electronics (cables, amplifiers, filters etc.) between it and the digitiser. A reference beam towards the calibrator for self-holography, $r_{\tau\eta\nu}$, can then be formed with these voltages by Eq.1.

$$r_{\tau\eta\nu} = z_{\tau\eta\nu} v_{\tau\eta\nu}. \quad (1)$$

The tensor of complex weights required to phase the telescope beam towards the calibrator source at each time step τ is $z_{\tau\eta\nu}$. Once the reference beam is formed, the measured correlations $h_{\eta\nu}$ can be computed by Eq.2.

$$h_{\eta\nu} = r^*_{\tau\eta\nu} v_{\tau\eta\nu} z_{\tau\eta\nu}. \quad (2)$$

It may be noted that in Eq.2, the lack of time index τ in the LHS denotes a *summation* over that index. In writing Eqs.1 and 2 we have departed from the convention followed in [5] and adopted a simpler convention that can be easily implemented using functions such as `einsum` available in the `numpy` package [7].

The measured correlations $h_{\nu\eta}$ are a product of the frequency dependent antenna gains (i.e. bandpasses) and the spectrum of the calibrator source. Therefore, by dividing these measured correlations with the calibrator flux density, the complex antenna bandpasses can be obtained. This makes broadband self-holography a simple way to calibrate large-N all-digital phased arrays such as the SKA-Low stations, without performing antenna-antenna cross-correlations to obtain visibilities. If visibilities are available, for example as UVFITS files, self-holography can be performed with them as well [5], using Eq.3.

$$h_{\nu\eta} = z_{\tau\nu\eta} c_{\tau\nu\eta\chi} z^*_{\tau\nu\chi}. \quad (3)$$

where $c_{\tau\nu\eta\chi}$ is the complex visibility between antennas numbered η and χ, for each frequency channel ν and time step τ. It may be noted that Eq.3 is provided only for reference. Although in later sections of this paper we compute visibilities for data diagnostics they are not used for self-holography.

3 Broadband self-holography applied to the EDA2

We tested broadband holography using data from the EDA2 with the Sun as the calibrator. The data were collected on Feb 06, 2024 around 13:15 AWST when the Sun was near the zenith. For about 3 minutes, 4096 raw voltage samples from all the 256 antennas and two polarisations sampled by the tile processing modules' (TPMs, [8]) ADCs were dumped into `hdf5` files each second. These samples are at the highest time cadence corresponding to 800 MSPS of sampling rate and have not undergone any signal processing within the TPMs. Also, this specific mode of data collection with the TPMs is intended primarily for diagnostics and not for regular operations.

For each time step, frequency dependent complex weights $z_{\tau\nu\eta}$ for steering the beam towards the Sun are computed using the known antenna locations and the position of the

Sun computed with `astropy` [10, 11, 12] using the timestamps in the data. These raw voltage data are then Fourier transformed to obtain 512 channels across 400 MHz. Reference beams are formed per Eq.1, the measured correlations are computed using Eq.2 and the resulting correlations are divided with a model of the Sun flux density [13]. The FFT, beamforming and computation of h are carried out with a NVIDIA GeForce GTX 750 GPU using the `cupy` package [9] and copied back to the host as `numpy` arrays, since the use of a GPU improves the speed of these steps.

We also cross-correlated and averaged the Fourier transformed data with the GPU using `cupy`, resulting in a $256 \times 256 \times 512 \times 4$ multi-frequency visibility cube which can be used for various diagnostics such as imaging. In Fig.1, the autocorrelations of the two orthogonal polarisations XX and YY averaged across antennas and time are shown. The averaged autocorrelations show some RFI in the ~136 MHz Orbcomm, ~250 MHz FLTSATCOM/UFO and ~370 MHz MUOS satellite downlink bands.

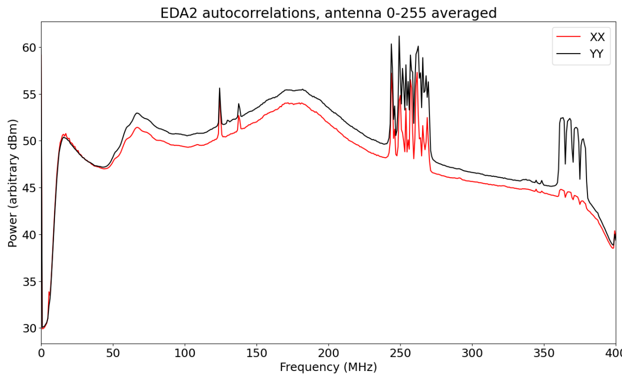

Figure 1. Time and antenna averaged autocorrelations.

In Fig.2, the average of bandpasses of the first 10 antennas for both the polarisations are shown. It may be noted that these bandpasses from holography include the effects of the antenna beam. In the same figure, the bandpasses derived using the standard EDA2 calibration loop performed around 13:50 AWST on the same day are also shown. This calibration loop - which is independent of the self-holography algorithm - involves sweeping across all the 512 coarse channels of the TPMs to collect visibilities and calibration with `mfcal` task in `miriad`, and takes about 20 to 30 minutes to complete [14]. Fig.2 shows good agreement between bandpasses obtained with self-holography and `mfcal` in the 50-350 MHz range where the EDA2 antennas are most sensitive. It is also interesting to note the minimal effect RFI has on the holography derived bandpasses.

In Fig.3, a comparison of the phases obtained with self-holography and `mfcal` for a selected few antennas is shown. The phases derived from the two different techniques are similar, and in both the cases the phases within the passband show linear trends with frequency denoting

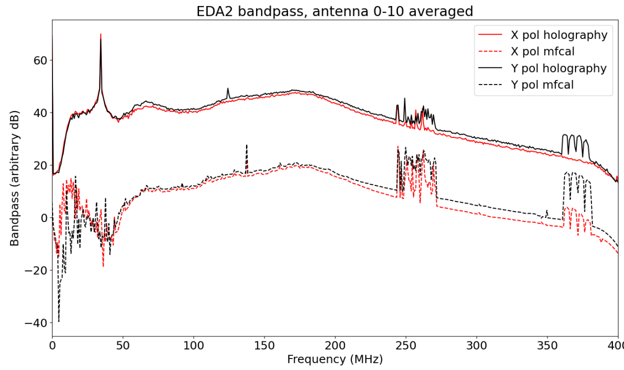

Figure 2. Average bandpasses of antennas 0 to 10. The bandpasses derived from `mfcal` have a different overall scaling to holography and are therefore offset in this figure.

differential delays between the antennas, for example due to cable length differences. These phases can be fitted with a linear model to derive the individual antenna delays. Since the phases are consistent between `mfcal` and self-holography, the delays derived are also expected to be similar.

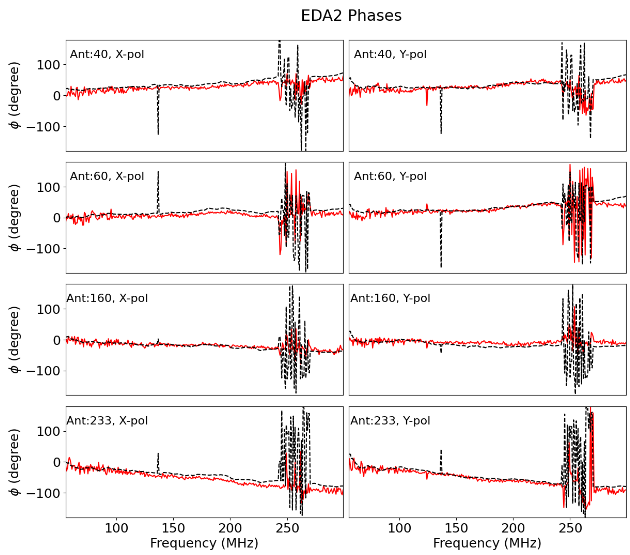

Figure 3. A comparison of self-holography derived phases (red) with `mfcal` phases (black) for a selected few antennas. The phases show linear trends and are remarkably similar between the two different techniques.

4 Conclusions and future work

As we have shown in this paper, broadband self-holography is a simpler alternative to the swept frequency station calibration loop. While the frequency sweep calibration loop requires cross-correlation between all the antennas and takes considerable amount of time, self-holography can be performed with raw voltage dumps and a few linear algebra operations. This makes it easy to implement as a real-time calibration method, and can be implemented in the FPGAs used for channelisation. The position of the Sun can be tabulated and stored as a look up table (LUT). However, due to the use of a diagnostic mode of TPMs which bypasses the signal processing firmware, the bandpasses shown in this paper do not include the effects of channelisation and therefore cannot be directly used to calibrate the data. Besides, due to data rate limitations, only 4096 samples out of 800 million sampled each second go into self-holography leading to lower SNRs. These two limitations can be partially mitigated with dumps of channelised voltages from the TPMs, although at present the TPM firmware does not provide all the channels synchronously in that mode. Also, the self-holography presented in this paper does not account for the EEPs of the individual antennas. While this is expected to be minimal for EDA2 due to its lower levels of mutual coupling, it cannot be ignored for SKA-Low stations [15].

5 Acknowledgements

This work makes use of Inyarrimanha Ilgari Bundara (Murchison Radio-astronomy Observatory), operated by CSIRO. We acknowledge the Wajarri Yamatji people as the traditional owners of the Observatory site. EDA2 is hosted by the Murchison Widefield Array under an agreement via the MWA External Instruments Policy. We acknowledge the efforts of INAF in providing TPMs for EDA2. The acquisition systems for EDA2 were designed and purchased by INAF/Oxford University and the receiver chain was design by INAF, as part of the SKA design and prototyping program. This works also makes use of the NASA Astrophysics Data System (ADS).

In addition to the python packages mentioned in the main text, this work also uses the following packages and we would like to thank the authors and maintainers of these packages - `matplotlib` [16], and `h5py` (https://www.h5py.org/).

References

[1] S. J. Wijnholds, "Calibration of mid-frequency aperture array stations using self-holography", *Proc. Int. Conf. Electromagn. Adv. Appl. (ICEAA)*, pp. 967-970, Sep. 2017

[2] U. Kiefner, R. B. Wayth, D. B. Davidson, and M. Sokolowski, "Holographic Calibration of Phased Array Telescopes," *Radio Science*, **vol. 56**, no. 5. American Geophysical Union (AGU), Apr. 29, 2021. doi: 10.1029/2020rs007171.

[3] C. R. Wilke, S. J. Wijnholds, and J. Gilmore, "Calibratability of Aperture Arrays Using Self-Holography," *IEEE Transactions on Antennas and Propagation*, **vol. 69**, no. 8. Institute of Electrical and Electronics Engineers (IEEE), pp. 4527–4537, Aug. 2021. doi: 10.1109/tap.2021.3060070.

[4] C. R. Wilke, S. J. Wijnholds, and J. Gilmore, "Calibratability of mid-frequency aperture arrays with self-holography," *Journal of Astronomical Telescopes, Instruments, and Systems*, **vol. 8**, no. 01. SPIE-Intl Soc Optical Eng, Nov. 19, 2021. doi: 10.1117/1.jatis.8.1.011008.

[5] Thekkeppattu, J. N., Wayth, R. B., and Sokołowski, M., "Calibration of an SKA-Low Prototype Station Using Holographic Techniques", *Radio Science*, **59**, no. 1, Art. no. e2023RS007847, Wiley, 2024. doi:10.1029/2023RS007847.

[6] R. Wayth et al., "Engineering Development Array 2: design, performance, and lessons from an SKA-Low prototype station," *Journal of Astronomical Telescopes, Instruments, and Systems*, **vol. 8**, no. 01. SPIE-Intl Soc Optical Eng, Dec. 20, 2021. doi: 10.1117/1.jatis.8.1.011010.

[7] Harris, C.R., Millman, K.J., van der Walt, S.J. et al. "Array programming with NumPy". *Nature* **585**, 357–362 (2020). https://doi.org/10.1038/s41586-020-2649-2

[8] G. Naldi et al., "The Digital Signal Processing Platform for the Low Frequency Aperture Array: Preliminary Results on the Data Acquisition Unit," *Journal of Astronomical Instrumentation*, **vol. 06**, no. 01. World Scientific Pub Co Pte Ltd, Mar. 2017. doi: 10.1142/s2251171716410142.

[9] Okuta, R., Unno, Y., Nishino, D., Hido, S., and Loomis, C., "CuPy: A NumPy-Compatible Library for NVIDIA GPU Calculations", *Proceedings of Workshop on Machine Learning Systems (LearningSys) in The Thirty-first Annual Conference on Neural Information Processing Systems (NIPS)*, (2017). http://learningsys.org/nips17/assets/papers/paper_16.pdf

[10] The Astropy Collaboration, "Astropy: A community Python package for astronomy," *Astronomy & Astrophysics*, **vol. 558**. EDP Sciences, p. A33, Sep. 30, 2013. doi: 10.1051/0004-6361/201322068.

[11] The Astropy Collaboration, "The Astropy Project: Building an Open-science Project and Status of the v2.0 Core Package," *The Astronomical Journal*, **vol. 156**, no. 3. American Astronomical Society, p. 123, Aug. 24, 2018. doi: 10.3847/1538-3881/aabc4f.

[12] The Astropy Collaboration, "The Astropy Project: Sustaining and Growing a Community-oriented Open-source Project and the Latest Major Release (v5.0) of the Core Package," *The Astrophysical Journal*, **vol. 935**, no. 2. American Astronomical Society, p. 167, Aug. 01, 2022. doi: 10.3847/1538-4357/ac7c74.

[13] A. O. Benz, "Radio Emission of the Quiet Sun," *Landolt Börnstein*, **4B**, 103 (2009).

[14] M. Sokolowski et al., “A Southern-Hemisphere all-sky radio transient monitor for SKA-Low prototype stations,” *Publications of the Astronomical Society of Australia*, **vol. 38**. Cambridge University Press (CUP), 2021. doi: 10.1017/pasa.2021.16.

[15] P. Bolli, M. Bercigli, P. Di Ninni, L. Mezzadrelli, and G. Virone, “Impact of mutual coupling between SKALA4.1 antennas to the spectral smoothness response,” *Journal of Astronomical Telescopes, Instruments, and Systems*, **vol. 8**, no. 01. SPIE-Intl Soc Optical Eng, Feb. 25, 2022. doi: 10.1117/1.jatis.8.1.011023.

[16] J. D. Hunter, "Matplotlib: A 2D Graphics Environment," *Computing in Science & Engineering*, **vol. 9**, no. 3, pp. 90-95, May-June 2007, doi: 10.1109/MCSE.2007.55